ACS Photonics

pubs.acs.org/journal/apchd5

Article

Arbitrary-Charged Weyl Points in One-Dimensional Helical Photonic Crystals

Guan-Run Wang, Wei-Min Deng, Wen-Jie Chen,* and Jian-Wen Dong*

Cite This: https://doi.org/10.1021/acsphotonics.5c01105

Read Online

ACCESS | Metrics & More | Article Recommendations | Supporting Information

ABSTRACT: The exotic physical properties of the Weyl points are mainly determined by their topological charges. Protected by crystallographic symmetries, Weyl charges on highly symmetric points can be larger than 1, termed multiple Weyl points. However, for all types of 3D crystals with 230 space groups, the orders of (screw) rotation axes can only be 1, 2, 3, 4, or 6, limiting the maximal Weyl charge of a natural 3D material to be 4. Here, we demonstrate that arbitrary-charged Weyl points can be stabilized in a 1D helical photonic crystal. Moreover, we give a complete theoretical analysis of all types of 1D HPCs and multiple Weyl points therein. Our findings offer a generally applicable strategy for designing arbitrary-ordered axes and realizing arbitrary-charged Weyl points in classical wave systems.

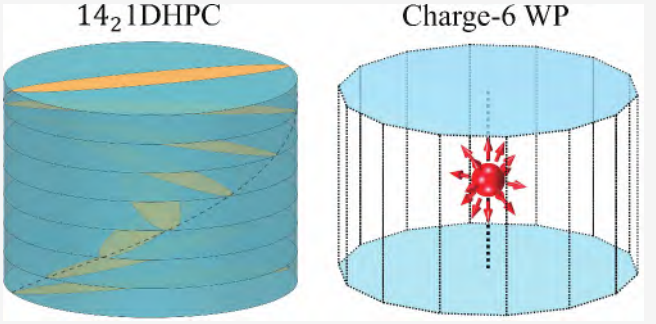

KEYWORDS: *photonic crystals, topological photonics, Weyl points, screw symmetry, anisotropic medium*

INTRODUCTION

A longstanding issue in topological physics is exotic band degeneracies, such as Weyl points (WPs), Dirac points, nodal lines and their variants.[1−5] Among these 3D band degeneracies, WPs are the more fundamental one, whose existence requires only the translational symmetry of the lattice.[6] Acting as monopoles of the Berry curvature field (magnetic flux in momentum space), WPs can be characterized by Chern number on a sphere enclosing it.[7] Their topological charge guarantees the existence of helicoid surface states that consist of open arcs connecting the projection of WPs on the surface Brillouin zone.[8] So far, WPs have been experimentally observed in electric,[9] cold-atomic,[10] acoustic,[11,12] and photonic systems,[13] which inspires more works to discuss their potential applications, including optical cloaking,[14] chiral optical tweezers,[15] subwavelength passive optical isolators,[16] and so on. Essentially, many properties of Weyl crystals are determined by WP's topological charge, such as multihelicoid surface states,[17] quantized circulation of spatial shift of reflection beam,[18] topologically protected electromagnetic pulling forces,[19] and topological circular dichroism.[20]

Therefore, how to realize a WP with more topological charges has been a crucial problem in topological physics. In principle, crystallographic symmetries can bring together two or more single WPs onto a high-symmetry k-point forming a double or multiple WP.[21] A complete characterization has been performed to summarize WPs that can be achieved in all possible types of 3D crystals (with 230 space groups), concluding that the maximal charge number of a WP is 4.[22,23] The reason is that a multiple WP with higher topological charges is usually stabilized by higher (screw) rotation symmetries. However, crystallography told us that the orders of (screw) rotation axes in a 3D crystal can only be 1, 2, 3, 4, or 6, which limits the maximal Weyl charge in a natural 3D material. One approach to circumvent this problem is to introduce additional accidental/hidden symmetries (for instance, by fine-tuning the long-range interactions) constraining the WPs' positions in k-space.[24] This inevitably makes the system rather complicated or time-reversal symmetry (TRS) broken.

In this Article, we propose a scheme to realize arbitrary-charged WP using a simple 1D layered structure. Different from the 3D lattice structure, its basic constituents are homogeneous layered media possessing continuous translational symmetry in the $x-y$ plane. The layers are only periodically repeated in the z direction, making it compatible with an arbitrary rotation or a screw rotation axis (not limited to 1, 2, 3, 4, or 6). By stacking anisotropic dielectric layers with their major axes tracing out a helix in space, we theoretically studied the 3D band structures of these 1D helical photonic crystals (1D HPCs). Protected by its high ordered screw

Received: May 17, 2025
Revised: September 21, 2025
Accepted: September 23, 2025

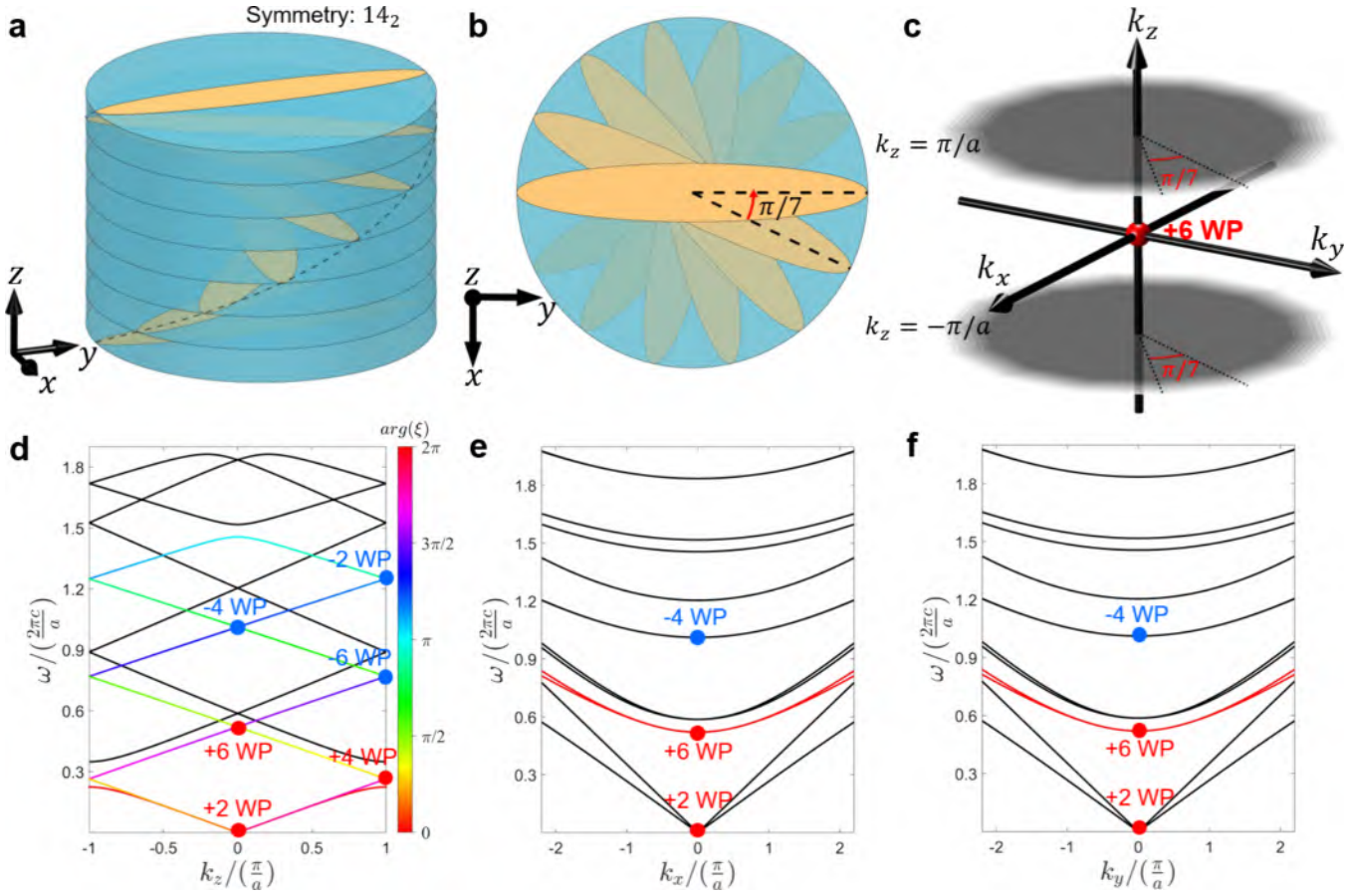

Figure 1. 1D HPC with a Chagre-6 WP. (a, b) Isometric view and bird's-eye view of a 1D HPC with 14_2 screw symmetry. The crystal is composed of 7 layers of anisotropic medium with identical principal dielectric constants but oriented in different directions. Each orange ellipse denotes the index ellipsoid of the layer. Their major axes trace a helix in space (dashed line). (c) 3D BZ of the 1D HPC. The BZ is bounded in the k_z direction by two planes (gray) of $k_z = \pm\pi/a$, but is infinite in plane because of continuous translation symmetry of layer medium. Due to 14_2 screw symmetry and TRS, this 3D BZ has a C_{14} rotation symmetry. (d–f) Bulk dispersion of a 1D HPC. A charge-6 WP resides at the BZ center between the 3rd and 4th bands. Screw eigenvalues of the lowest 7 bands are shown by the color codes in (d).

symmetry and TRS, WP with an arbitrary charge can be constructed at time-reversal invariant momenta (TRIM). Paradigmatically, we first study a 1D HPC with a 14-ordered (14_2) screw symmetry using a characteristic matrix method. A chagre-6 WP is found at the Γ point analyzed via its effective Hamiltonian and protected surface states. By considering 1D HPC with a higher-ordered screw axis, WPs with an arbitrary charge can in principle be obtained. Furthermore, in a 1D HPC with continuous screw rotation symmetry (the extreme case of discrete screw symmetry), the degenerate frequencies and topological charges of WPs at TRIM are proportional to the band numbers involved, which then have no upper bound.

RESULTS AND DISCUSSION

1D Helical Photonic Crystal with a Chagre-6 WP. As an example, we first consider a 1D HPC with a 14_2 screw symmetry. Its unit cell is composed of 7 layers with equal thickness, as depicted in Figure 1a,b. All these layers are uniaxial medium with identical principal dielectric constants $\varepsilon_1 = 2$, $\varepsilon_2 = 5$, and $\varepsilon_3 = 2$, but are oriented in different directions. Each two neighboring layers have a $\pi/7$ rotation, whose major axes form an RH helix in space. Permittivity tensors of the n^{th} layer can be obtained by a unitary transform, $\vec{\varepsilon}(\theta) = \vec{R}(\theta)\, diag(\varepsilon_1, \varepsilon_2, \varepsilon_3)\vec{R}^{-1}(\theta)$, where $\theta = (n-4) \times \pi/7$ ($1 \le n \le 7$, $n \in N$), and

$$\vec{R}(\theta) = \begin{bmatrix} \cos\theta & -\sin\theta & 0 \\ \sin\theta & \cos\theta & 0 \\ 0 & 0 & 1 \end{bmatrix} \quad (1)$$

Due to discrete translation symmetry along the z direction, the Brillouin zone (BZ) of 1D HPC [Figure 1c] is bounded by two flat planes (gray) $k_z = \pm\pi/a$. Meanwhile, it is infinite in the k_x–k_y plane because of continuous translational symmetry of the layer medium. As a result of the 14_2 screw symmetry and TRS, this 3D BZ and the corresponding bulk dispersion have a C_{14} rotation about the z-axis.

Here we calculate HPC's bulk band structure using a characteristic matrix method.[25,26] Bloch theorem requires that

$$\prod_{i=1}^{7} \vec{M}_i(\omega, k_x, k_y)[E_{xi}\, E_{yi}\, H_{xi}\, H_{yi}]^T = e^{ik_z a}[E_{xi}\, E_{yi}\, H_{xi}\, H_{yi}]^T \quad (2)$$

where $\vec{M}_i$ is the 4×4 characteristic matrix of the i^{th} layer. The $[E_{xi}E_{yi}H_{xi}H_{yi}]$ are tangential electric/magnetic fields on the bottom surface of the unit cell,[25] a is the lattice constant in the z-direction, and k_z is the Bloch wavenumber limited to $[-\pi, \pi]$. (A detailed derivation of $\vec{M}_i$ can be found in Materials and Methods and Supplementary 1.)

https://doi.org/10.1021/acsphotonics.5c01105
ACS Photonics XXXX, XXX, XXX−XXX

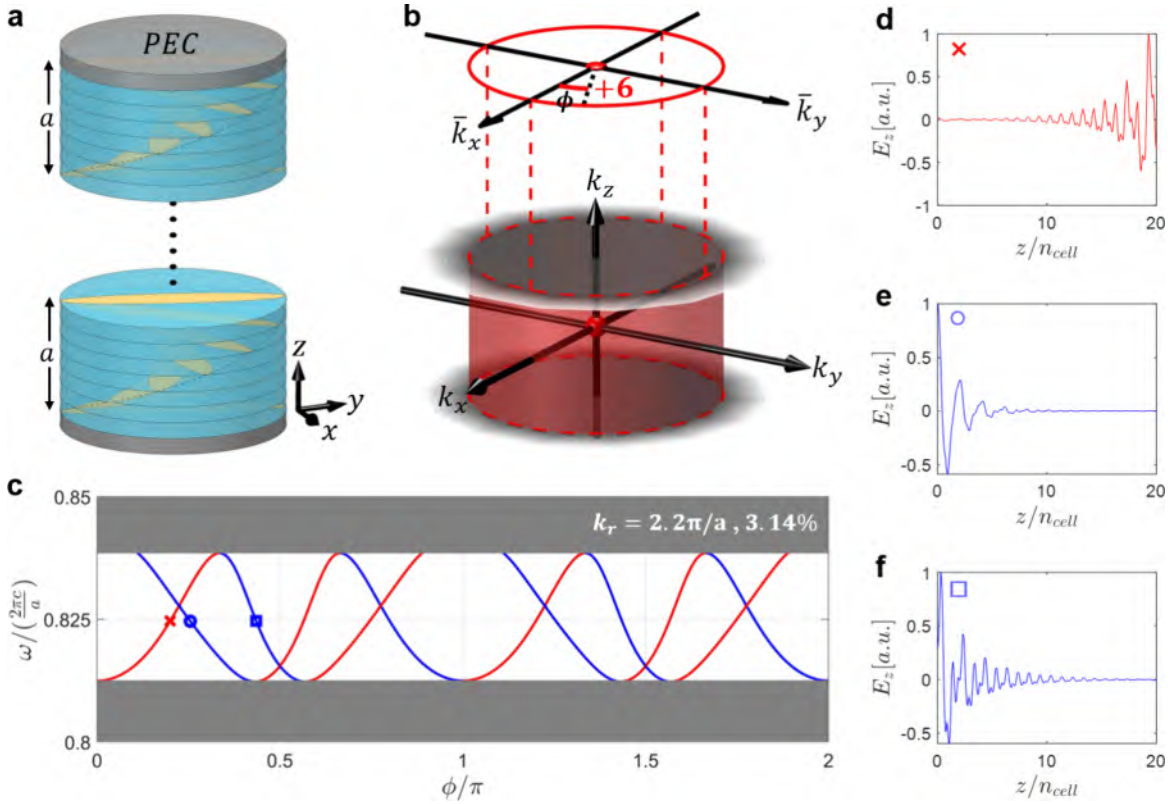

Figure 2. Sextuple helical surface states near the charge-6 WP. (a) Schematic of a 1D HPC with 20 periods sandwiched between PEC boundaries in the z-direction. (b) 3D bulk BZ and its surface projection on the k_x−k_y plane. Surface dispersion is calculated on a circle (red) enclosing WP, with a radius of $k_r = 2.2\pi/a$. Corresponding bulk states are on a tube in 3D bulk BZ. (c) Surface band dispersion on the red circle in (b). For both surfaces in (a), 6 gapless surface bands transverse the partial gap near charge-6 WP. Red (blue) lines plot the surface bands for the top (bottom) surface of the crystal. (d−f) Three representable E_z profiles of the surface modes marked by ×, ○, and □ in (c).

Calculated bulk dispersions in the k_x, k_y, and k_z directions are plotted in Figure 1d−f. As shown in Figure 1(d), the lowest 14 bands form a connected group because of 14_2 screw symmetry on the k_z axis. These bands fold back and forth between Γ and A, forming 6 linear crossing points at TRIM. By examining the dispersions nearby and k dot p Hamiltonians, we find that they are actually multiple WPs. Their topological charges can be evaluated by inspecting the screw eigenvalues ξ of the crossing bands.[21] In a screw-symmetric crystal, screw eigenvalues of the bulk bands are k_z-dependent

$$\xi = e^{-i(k_z a + p\pi)/7} \tag{3}$$

and their arguments evolve linearly along the screw invariant axis (k_z axis),[27,28] as color coded in Figure 1d. The integer $p \in \{1,3,5,7,9,11,13\} mod 14$ labels the bands with different rotation eigenvalues in a connected group[29] (see Supplementary 3 and 10). Specially at TRIM, since two crossing bands are related by TRS ($\hat{T}$ **E** = **E***), which requires TRS-related states to be mutual complex conjugates, their screw eigenvalues form a complex conjugate pair ($p_1 = -p_2$). Therefore, for each crossing point in Figure 1d, the argument difference between two crossing bands should be

$$\arg(\xi_2/\xi_1) = \frac{(p_1 - p_2)\pi}{7} = \pm 2l\frac{\pi i}{7} \quad (l = 1, 2, 3) \tag{4}$$

which has only six possible values. As discussed in Supplementary 3, WP's topological charge is proportional to the argument difference between two crossing bands, concluding the topological charges of WPs are even numbers,[30] and the maximal Weyl charge hosted in this 14_2 HPC is 6 (l = 3). Because TRS maps a WP at **k** to −**k** with the same chirality,[31] identical WPs always come in pairs on the k_z axis, except at TRIM. Likewise, for other types of 14-ordered HPCs with other translation indices, the charge of WPs at TRIM are also determined by 6 possible ratios of screw eigenvalues, and similar results can be obtained (see Supplementary 4).

Note that these charge-6 WPs go beyond the maximal Weyl charge (4) in 3D crystals.[23] For instance, the WP at the Γ point with frequency of $f = 0.52(c/a)$ [red dots in Figure 1d−f] is a charge-6 WP, which has a linear dispersion along the k_z axis but a quadratic dispersion along the in-plane directions. Its 2 × 2 low-energy effective Hamiltonian around Γ reads: (see Supplementary 3)

$$H(q) = (c_0 + c_2 q^2)\sigma_0 + a q_z \sigma_z + b(q_-^6 \sigma_+ + q_+^6 \sigma_-) \tag{5}$$

where a, b, c_0, and c_2 are real coefficients, $q^2 = q_+q_- + q_z^2$, $q_\pm = q_x \pm iq_y$, and $\sigma_\pm = \sigma_x \pm i\sigma_y$. This Hamiltonian, which has been discussed in many previous theoretical works,[32−34] is a general form of a charge-n WP (n = 6) and now has a feasible real structure.

Remarkably, the in-plane dispersion of charge-6 WP is k^2-type rather than k^6-type on the $k_z = 0$ plane. The reason is that the in-plane dispersion is dominated by the nonchiral quadratic term $(c_0 + c_2 q^2)\sigma_0$ in eq 5, which masks the sextuple dispersion from the chiral term $b(q_-^6\sigma_+ + q_+^6\sigma_-)$. The effect of the sextuple chiral term is manifested in the frequency difference between the two bands, which is almost invisible around the Γ point [Figure 1e,f] (see Supplementary 5). Thanks to the fact that

https://doi.org/10.1021/acsphotonics.5c01105
ACS Photonics XXXX, XXX, XXX−XXX

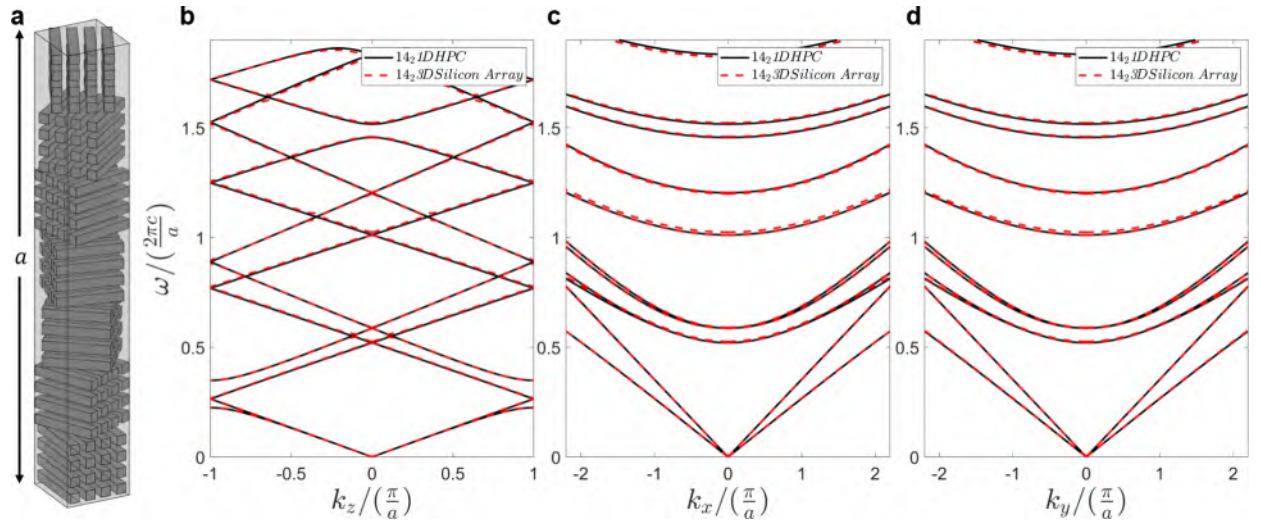

Figure 3. 1D HPC made up of silicon wire media. (a) Tetragonal supercell (with the size of $4w \times 4w \times a$) used in calculating the band structure of HPC. $w = a/28$ is the lattice constant of the wire array. (b–d) Bulk dispersions of to the HPC in x-, y-, and z-directions. It agrees well with the bulk bands (red dashed lines) of 1D HPC made up of uniaxial effective media ($\varepsilon_y = 5$, $\varepsilon_x = \varepsilon_z = 2$).

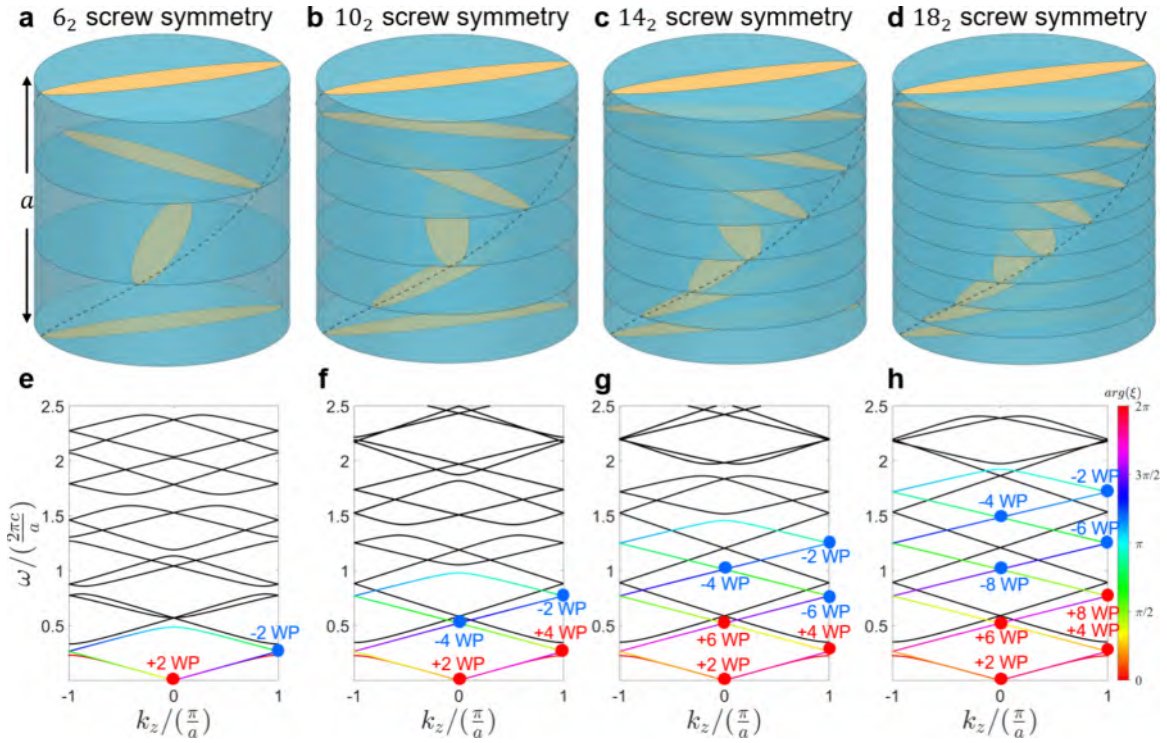

Figure 4. WPs stabilized by $(4n + 2)_2$ screw symmetry and TRS. (a–d) Isometric view of the unit cells with $(4n + 2)_2$ screw symmetries (n = 1, 2, 3, 4). (e, f) Corresponding bulk dispersions along k_z (screw axis). The maximal Weyl charge that can be stabilized in each case is $2n$. Screw eigenvalues of the first band group are shown by color codes.

1D HPC's BZ is infinite in the $k_x - k_y$ plane, the topological feature (Berry flux and resultant Fermi-arc states) of this charge-6 WP can be observed at large k_r.

Topological Features of Charge-6 WP. We truncate the HPC in the z direction, resulting in a slab, and cap the two truncated surfaces with two PECs [Figure 2a], which serves as a topologically trivial gap material. The 3D bulk BZ of the 1D HPC and its surface projection on the k_x–k_y plane is shown in Figure 2b. Considering the bulk-edge corresponding relation, the band dispersion in a tube oriented in the k_z direction of the 3D BZ reflects its Chern number. We give the surface-projected dispersion along a loop enclosing WP (red), with a radius of $k_r = 2.2\pi/a$ [Figure 2c], in which the red (blue) lines plot the surface bands for the top (bottom) surface. For each surface, 6 gapless surface bands with positive (negative) slopes traverse the partial band gap (relative bandwidth is 3.14%), reflecting the sextuple topological charge. Because of its truncation in the z-direction, HPC's 14_2 screw symmetry is broken. However, the C_{2i} ($i = x, y, z$) rotation symmetry and TRS are preserved. For this reason, 12 surface bands (6 on top surface and 6 on bottom surface) are related with each other. Figure 2d–f plots the eigen fields (E_z) of three representative

https://doi.org/10.1021/acsphotonics.5c01105
ACS Photonics XXXX, XXX, XXX–XXX

surface modes (denoted by ×, ○, and □). These surface modes can be excited by oblique incident beams through a conical prism (see Supplementary 6). Despite lacking complete bandgap, the system exhibits partial bandgaps at a specific k_r (e.g., at $k_r = 2.2\pi/a$, say, for a fixed incident angle) enable topological insulation along ϕ, suggesting potential applications in chiral sensors.[35] Topological features of the charge-6 WP can also be examined by its Berry Curvature distribution and the Berry Phase evolution around it (see Supplementary 2).

Realize 1D HPC by Silicon Wire Medium Array. In the above calculation, the birefringence $\varepsilon_2/\varepsilon_1 = 2.5$ is somehow unrealistic in nature. Physically, such a kind of anisotropic material can be realized by a finely stratified medium[36−38] or dielectric wire medium[39,40] composed of two isotropic materials. By replacing each anisotropic layer with a silicon wire array, we construct a meta HPC in Figure 3a. The band structures of silicon wire array were calculated by MPB using a supercell with size of $(a_x, a_y, a_z) = \left(\frac{a}{7}, \frac{a}{7}, a\right)$, see Figure 3b−d. The dielectric constant and refractive index of silicon are $\varepsilon = 12$ and $n = 3.464$. The in-plane lattice constant of the silicon wire is $w = a/28$. Each silicon wire features a square cross-section with a side length of $(2 - \sqrt{2})w$. For the modes in the lowest two connected groups, the silicon wires have feature sizes much smaller than the wavelength, acting as a good effective medium. Corresponding band structures (dashed lines in Figure 3b−d) coincide with the one made up of homogeneous medium (solid lines in Figure 3b−d). Due to its subwavelength feature, the effective medium works well even with misalignment of wires (see Supplementary 7). Furthermore, due to the robustness of Weyl charges in the k space, moderate perturbation of birefringence and disorder of the screw periodicity would not disrupt the existence of helical surface states (see Supplementary 8). All of these results imply that the topological feature of this 1D HPC could be observed using current nanofabrication techniques.

Higher-Charged WPs Stabilized by Higher-Ordered Screw Symmetry. Since each anisotropic medium layer has continuous translational symmetry and C_2 rotation symmetry in the x−y plane, 1D HPC can have an arbitrary-ordered screw axis, even that it is not compatible with 3D crystallographic lattice. This makes arbitrary-charged Weyl degeneracies achievable in a simple 1D structure. For an HPC composed of anisotropic dielectrics, the system possesses C_2 rotation, $2N_{2q}$ screw rotation, and TR symmetries. Other than the in-plane continuous translations and TR, HPC's symmetry can be described by a $2N_{2q}22$ rod group,[41] where q and N are integers $(q < N)$.

For the sake of limited possible screw rotation eigenvalues constrained by the 14_222 rod group and TR, the maximal Weyl charge hosted by a 14_2 HPC is 6. One can infer that HPC with a higher-ordered screw axis can host higher-charged WP. Figure 4a−d exemplifies the cases of 6_2, 10_2, and 18_2 HPCs (the cases for even order of N will be discussed later). As expected, the $(4n + 2)_2$ screw symmetry combines $N = 2n + 1$ bands into a connected group, resulting in $2n$ crossing points at TRIM. Constrained by TRS, the rotational eigenvalues of two crossing bands are a complex conjugate pair. The ratio between them must be $e^{\pm 2m\pi i/2n+1}$ $(m = 1, 2, ..., n)$. And the topological charge of WP can only be an even number less than $2n$. Effective Hamiltonian near a charged-$2m$ WP takes a similar form as eq 5 (see Supplementary 3):

$$H(q) = (c_0 + c_2q^2)\sigma_0 + aq_z\sigma_z + b(q_-^{2m}\sigma_+ + q_+^{2m}\sigma_-) \quad (6)$$

where $m \leq n$. Obviously, higher screw symmetry can protect the larger Weyl charge. In principle, we can realize an arbitrary-charged WP in an HPC with a large enough order $2N$.

For the case of an even $N = 2n$, the maximal charge protected by HPC's symmetry is N. This can be derived through an effective Hamiltonian analysis similar to above. Figure 5 exemplifies the HPCs with 4_222, 8_222, 12_222, and

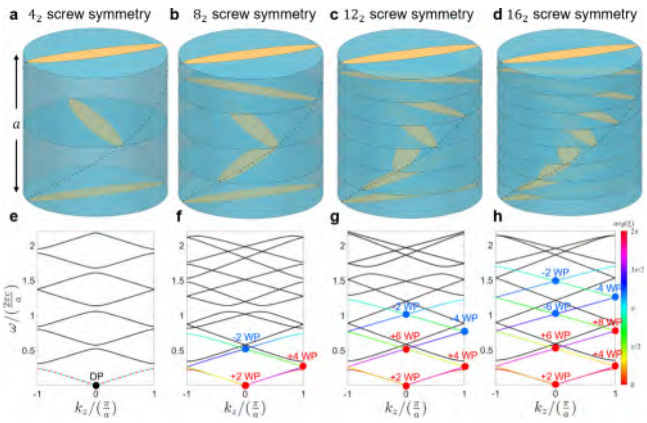

Figure 5. WPs stabilized by $4n_2$ screw symmetry and TRS. (a−d) Isometric view of the unit cells with $4n_2$ screw symmetries (n = 1, 2, 3, 4). (e, f) Corresponding bulk dispersions along k_z (screw axis). The maximal Weyl charge that can be stabilized in each case is $2n$.

16_222 rod group. In particular, the 4_2 HPC possesses inversion symmetry and is a nonchiral structure. Thus, each band in Figure 5e is a double band, and WP disappears. Overall, an HPC with higher screw axis can host a larger Weyl degeneracy. The maximal charge for an HPC with $2N$-ordered screw symmetry can be summarized as

$$C_{\max} = \begin{cases} N - 1 & (N = 2n + 1,\ n = 1, 2, 3, ...) \\ N & (N = 2n,\ n = 2, 3, 4, ...) \end{cases} \quad (7)$$

Furthermore, it is interesting to consider the extreme case when N approaches to infinity. Then the $2N$-ordered screw axis becomes a continuous screw axis, and this 1D HPC with continuous screw axis coincidently has the same space group as cholesteric liquid crystals.[42] The permittivity tensor of this continuous 1D HPC can be written as

$$\vec{\varepsilon} = \begin{bmatrix} \varepsilon_1\cdot\cos^2\left(\frac{z\pi}{a}\right) + \varepsilon_2\cdot\sin^2\left(\frac{z\pi}{a}\right) & (\varepsilon_1 - \varepsilon_2)\cdot\cos\left(\frac{z\pi}{a}\right)\cdot\sin\left(\frac{z\pi}{a}\right) & 0 \\ (\varepsilon_1 - \varepsilon_2)\cdot\cos\left(\frac{z\pi}{a}\right)\cdot\sin\left(\frac{z\pi}{a}\right) & \varepsilon_1\cdot\sin^2\left(\frac{z\pi}{a}\right) + \varepsilon_2\cdot\cos^2\left(\frac{z\pi}{a}\right) & 0 \\ 0 & 0 & \varepsilon_3 \end{bmatrix} \quad (8)$$

where a is the period in z-direction. Its isometric view and calculated bulk dispersion along k_z are plotted in Figure 6a,b, where $\varepsilon_1 = \varepsilon_3 = 2$, $\varepsilon_2 = 5$.

Due to its highest screw rotation symmetry, each connected group in the band structure consists of an infinite number of bands folded forth and back between TRIMs. Note that a band gap is opened for the circular polarization with the same handedness as the HPC (more details in Supplementary 9). Meanwhile, all these folding points are WPs, whose charges are labeled in Figure 6b. As predicted by the screw eigenvalues, the

https://doi.org/10.1021/acsphotonics.5c01105
ACS Photonics XXXX, XXX, XXX−XXX

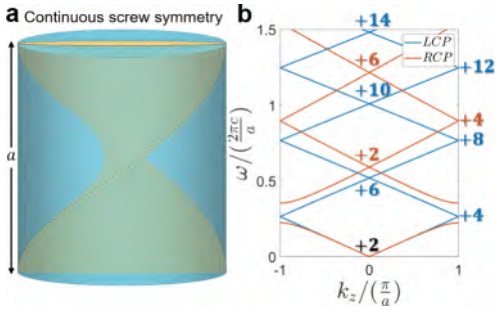

Figure 6. 1D HPC with continuous screw symmetry. (a) Isometric view of the unit cell. (b) Bulk dispersion along k_z (screw axis). Two sets of bands (red and blue, RCP and LCP) fold back and forth between the TRIMs. The Weyl charges monotonically increase as the frequency increases, and thus, Weyl charges have no upper bound in principle.

Weyl charges monotonically increase with frequency and do not have an upper bound (see Supplementary 10). In fact, the physical limitation to observe higher Weyl charges lies in the gap width associated with high frequency, which is determined by the effective anisotropy of dielectric wire array. However, if we extend the concepts to THz/microwave regime, we can use high ε dielectric or metal to construct HPC, higher Weyl charges could be observable.

CONCLUSIONS

In conclusion, we theoretically proposed and studied 1D layered HPCs composed of anisotropic dielectrics. Due to the continuous translation symmetry of layered medium, such type of HPC can have an arbitrary screw axis which can go beyond the 3D Bravais lattice. Weyl charges in this layered system can be bigger than 4, the maximal Weyl charge that can be host in a 3D crystal (with all of the possible 230 types of space group). Our work establishes a novel photonic platform for exploring exotic physical phenomena related to multiple WPs, such as quantized circular photogalvanic effect in Weyl semimetals[43] and quantized circulation of spatial shift in interface reflection.[18] Our work may inspire further research on applications of large charged Weyl medium, such as optical tweezers,[15] optical microcavity[44] and so on. In addition, our theory can be easily extended to other classical wave systems, including phononic crystals,[45] magnonic crystals[46] and electric circuits.[47]

MATERIALS AND METHODS

Characteristic Matrix Method of 1D HPC. Detailed derivation about the 4 × 4 characteristic matrix for anisotropic layer can be found in Supplementary 1.

Numerical Simulation. The surface states in Figure 2 were computed using COMSOL Multiphysics 5.6 by solving the eigenstates of a finite HPC bounded by PEC boundaries. To accurately model its continuous translational symmetry in the $x-y$ plane, we set the transverse unit cell dimension to be 1/20 of the longitudinal lattice constant a.

The band structures of HPC made up of silicon wire metamaterials [Figure 3a] were calculated by MIT Photonic Bands (MPB)[48] using a supercell with a size of $(a_x,a_y,a_z) = (a/7,a/7,a)$. The dielectric constant and refractive index of silicon are $\varepsilon = 12$ and $n = 3.464$. The in-plane lattice constant of silicon wire is $w = a/28$. Each silicon wire features a square cross-section with side length $(2-\sqrt{2})w$ of the pixel resolution used in MPB is $a/224$. Thus, the filling ratio of the structure is $(2-\sqrt{2})^2 = 34.3\%$. In addition, this type of HPC cannot find a simple unit cell because 14-sided polygons cannot tile a plane. Although some structural mismatches exist on the supercell boundaries, the resultant band structure should agree well with the ideal HPC made up of effective media, as long as the lateral size of the supercell is big enough.

ASSOCIATED CONTENT

Supporting Information

The Supporting Information is available free of charge at https://pubs.acs.org/doi/10.1021/acsphotonics.5c01105.

The derivation of the Characteristic Matrix Method (CMM), Berry Curvature distribution, and the Berry Phase evolution of charge-6 WP, low-energy effective Hamiltonians for charge-6 WP, 14-ordered 1D HPCs with different translation indices, the in-plane dispersion near a multiple WP, excitation of helical surface states, misalignment tolerance of 1D meta HPC, and the robustness of helical surface states, circular polarization gaps of 1D HPCs, and Weyl charge monotonically increasing with frequency (PDF)

AUTHOR INFORMATION

Corresponding Authors

Wen-Jie Chen − *Department of Physics and State Key Laboratory of Optoelectronic Materials and Technologies, Sun Yat-sen University, Guangzhou 510275, China;* orcid.org/0000-0003-3119-2220; Email: chenwenj5@mail.sysu.edu.cn

Jian-Wen Dong − *Department of Physics and State Key Laboratory of Optoelectronic Materials and Technologies, Sun Yat-sen University, Guangzhou 510275, China;* orcid.org/0000-0003-2379-554X; Email: dongjwen@mail.sysu.edu.cn

Authors

Guan-Run Wang − *Department of Physics and State Key Laboratory of Optoelectronic Materials and Technologies, Sun Yat-sen University, Guangzhou 510275, China*

Wei-Min Deng − *School of Physics and Materials Science and Jiangxi Provincial Key Laboratory of Photodetectors, Nanchang University, Nanchang 330031, China*

Complete contact information is available at: https://pubs.acs.org/10.1021/acsphotonics.5c01105

Author Contributions

W.-J.C. conceived the idea. G.-R.W., W.-J.C., and W.-M.D. derived the characteristic matrix method of 1D HPCs. G.-R.W. performed the numerical simulations. All authors contributed to the analysis of the results. G.-R.W., W.-J.C., and J.-W.D. wrote the manuscript. W.-J.C. and J.-W.D. supervised the project.

Funding

This work was supported by the National Natural Science Foundation of China (Grant No. 62035016); Guangdong Basic and Applied Basic Research Foundation (Grant No. 2023B1515040023); Natural Science Foundation of Jiangxi Province (Grant No. 20242BAB20023); Training Program for Academic and Technical Leaders of Major Disciplines in Jiangxi Province (Grant No. 20243BCE51163); and the

Fundamental Research Funds for the Central Universities, Sun Yat-sen University (Grant No. 24lgzy007).

Notes

The authors declare no competing financial interest.

■ ACKNOWLEDGMENTS

This work was supported by National Natural Science Foundation of China (Grant. No. 62035016), Guangdong Basic and Applied Basic Research Foundation (Grant No. 2023B1515040023), and the Fundamental Research Funds for the Central Universities, Sun Yat-sen University (Grant No. 24lgzy007). W.-M.D. was supported by Natural Science Foundation of Jiangxi Province (Grant No. 20242BAB20023) and Training Program for Academic and Technical Leaders of Major Disciplines in Jiangxi Province (Grant No. 20243BCE51163).

■ REFERENCES

(1) Armitage, N. P.; Mele, E. J.; Vishwanath, A. Weyl and Dirac semimetals in three-dimensional solids. *Rev. Mod. Phys.* **2018**, *90* (1), 015001.
(2) Lan, Z.; Chen, M. L. N.; Gao, F.; Zhang, S.; Sha, W. E. I. A brief review of topological photonics in one, two, and three dimensions. *Rev. Phys.* **2022**, *9*, 100076.
(3) Qu, T.; Wang, M.; Cheng, X.; Cui, X.; Zhang, R.-Y.; Zhang, Z.-Q.; Zhang, L.; Chen, J.; Chan, C. T. Topological Photonic Alloy. *Phys. Rev. Lett.* **2024**, *132* (22), 223802.
(4) Breitkreiz, M.; Brouwer, P. W. Fermi-Arc Metals. *Phys. Rev. Lett.* **2023**, *130* (19), 196602.
(5) Deng, W.-M.; Chen, Z.-M.; Li, M.-Y.; Guo, C.-H.; Tian, Z.-T.; Sun, K.-X.; Chen, X.-D.; Chen, W.-J.; Dong, J.-W. Ideal nodal rings of one-dimensional photonic crystals in the visible region. *Light Sci. Appl.* **2022**, *11* (1), 134.
(6) Fonseca, G. R.; Prudêncio, F. R.; Silveirinha, M. G.; Huidobro, P. A. First-principles study of topological invariants of Weyl points in continuous media. *Phys. Rev. Res.* **2024**, *6* (1), 013017.
(7) Soluyanov, A. A.; Gresch, D.; Wang, Z.; Wu, Q.; Troyer, M.; Dai, X.; Bernevig, B. A. Type-II Weyl semimetals. *Nature* **2015**, *527* (7579), 495−498.
(8) Fang, C.; Lu, L.; Liu, J.; Fu, L. Topological semimetals with helicoid surface states. *Nat. Phys.* **2016**, *12* (10), 936−941.
(9) Xu, S.-Y.; Belopolski, I.; Alidoust, N.; Neupane, M.; Bian, G.; Zhang, C.; Sankar, R.; Chang, G.; Yuan, Z.; Lee, C.-C.; et al. Discovery of a Weyl fermion semimetal and topological Fermi arcs. *Science* **2015**, *349* (6248), 613−617.
(10) Wang, Z.-Y.; Cheng, X.-C.; Wang, B.-Z.; Zhang, J.-Y.; Lu, Y.-H.; Yi, C.-R.; Niu, S.; Deng, Y.; Liu, X.-J.; Chen, S.; et al. Realization of an ideal Weyl semimetal band in a quantum gas with 3D spin-orbit coupling. *Science* **2021**, *372* (6539), 271−276.
(11) Li, F.; Huang, X.; Lu, J.; Ma, J.; Liu, Z. Weyl points and Fermi arcs in a chiral phononic crystal. *Nat. Phys.* **2018**, *14* (1), 30−34.
(12) Ge, H.; Ni, X.; Tian, Y.; Gupta, S. K.; Lu, M.-H.; Lin, X.; Huang, W.-D.; Chan, C. T.; Chen, Y.-F. Experimental Observation of Acoustic Weyl Points and Topological Surface States. *Phys. Rev. Appl.* **2018**, *10* (1), 014017.
(13) Lu, L.; Wang, Z.; Ye, D.; Ran, L.; Fu, L.; Joannopoulos, J. D.; Soljačić, M. J. S. Experimental observation of Weyl points. *Science* **2015**, *349* (6248), 622−624.
(14) Takahashi, S.; Tamaki, S.; Yamashita, K.; Yamaguchi, T.; Ueda, T.; Iwamoto, S. Transmission properties of microwaves at an optical Weyl point in a three-dimensional chiral photonic crystal. *Opt. Express* **2021**, *29* (17), 27127−27136.
(15) Yang, Y.; Chan, H.-C.; Bi, K.; Duan, G.; Liu, M.; Wang, H.; Li, L. Optical forces in photonic Weyl system. *New J. Phys.* **2022**, *24* (4), 043019.
(16) Asadchy, V. S.; Guo, C.; Zhao, B.; Fan, S. Sub-Wavelength Passive Optical Isolators Using Photonic Structures Based on Weyl Semimetals. *Adv. Opt. Mater.* **2020**, *8* (16), 2000100.
(17) He, H.; Qiu, C.; Cai, X.; Xiao, M.; Ke, M.; Zhang, F.; Liu, Z. Observation of quadratic Weyl points and double-helicoid arcs. *Nat. Commun.* **2020**, *11* (1), 1820.
(18) Liu, Y.; Yu, Z.-M.; Xiao, C.; Yang, S. A. Quantized Circulation of Anomalous Shift in Interface Reflection. *Phys. Rev. Lett.* **2020**, *125* (7), 076801.
(19) Liu, Y.; Wang, M.; Huang, Y.; Wang, G. P.; Zhang, S. Continuous evolution of Fermi arcs in a minimal ideal photonic Weyl medium. *Light Sci. Appl.* **2024**, *13* (1), 276.
(20) Ahn, J.; Ghosh, B. Topological Circular Dichroism in Chiral Multifold Semimetals. *Phys. Rev. Lett.* **2023**, *131* (11), 116603.
(21) Fang, C.; Gilbert, M. J.; Dai, X.; Bernevig, B. A. Multi-Weyl Topological Semimetals Stabilized by Point Group Symmetry. *Phys. Rev. Lett.* **2012**, *108* (26), 266802.
(22) Yu, Z.-M.; Zhang, Z.; Liu, G.-B.; Wu, W.; Li, X.-P.; Zhang, R.-W.; Yang, S. A.; Yao, Y. Encyclopedia of emergent particles in three-dimensional crystals. *Sci. Bull.* **2022**, *67* (4), 375−380.
(23) Chen, Q.; Chen, F.; Pan, Y.; Cui, C.; Yan, Q.; Zhang, L.; Gao, Z.; Yang, S. A.; Yu, Z.-M.; Chen, H.; et al. Discovery of a maximally charged Weyl point. *Nat. Commun.* **2022**, *13* (1), 7359.
(24) Biao, Y.; Yu, R. Realization of ideal unconventional Weyl states with arbitrary topological charge. *Phys. Rev. B* **2023**, *108* (16), 165128.
(25) Macleod, H. A. *Thin-Film Optical Filters*; CRC Press, 2017.
(26) Knittl, Z. k. *Optics of Thin Films; An Optical Multilayer Theory*; Wiley, 1976.
(27) Tsirkin, S. S.; Souza, I.; Vanderbilt, D. Composite Weyl nodes stabilized by screw symmetry with and without time-reversal invariance. *Phys. Rev. B* **2017**, *96* (4), 045102.
(28) Chang, M.-L.; Xiao, M.; Chen, W.-J.; Chan, C. T. Multiple Weyl points and the sign change of their topological charges in woodpile photonic crystals. *Phys. Rev. B* **2017**, *95* (12), 125136.
(29) Bliokh, K. Y.; Smirnova, D.; Nori, F. Quantum spin Hall effect of light. *Science* **2015**, *348* (6242), 1448−1451.
(30) Wang, X.; Zhou, F.; Zhang, Z.; Wu, W.; Yu, Z.-M.; Yang, S. A. Single pair of multi-Weyl points in nonmagnetic crystals. *Phys. Rev. B* **2022**, *106* (19), 195129.
(31) Lu, L.; Fu, L.; Joannopoulos, J. D.; Soljačić, M. Weyl points and line nodes in gyroid photonic crystals. *Nat. Photonics* **2013**, *7* (4), 294−299.
(32) Cerjan, A.; Xiao, M.; Yuan, L.; Fan, S. Effects of non-Hermitian perturbations on Weyl Hamiltonians with arbitrary topological charges. *Phys. Rev. B* **2018**, *97* (7), 075128.
(33) Zhang, T.; Takahashi, R.; Fang, C.; Murakami, S. Twofold quadruple Weyl nodes in chiral cubic crystals. *Phys. Rev. B* **2020**, *102* (12), 125148.
(34) González-Hernández, R.; Tuiran, E.; Uribe, B. Chiralities of nodal points along high-symmetry lines with screw rotation symmetry. *Phys. Rev. B* **2021**, *103* (23), 235143.
(35) Ye, H.-N.; Wan, B.-F.; Zhao, Y.-Q.; Li, B.-X.; Zhang, H.-F. Responsive refractive index sensor based on actively tuning liquid crystal topological edge states. *Phys. Fluids* **2024**, *36* (7), 077103.
(36) Rytov, S. Electromagnetic properties of a finely stratified medium. *Sov. Phys. JETP* **1956**, *2* (3), 466−475.
(37) Wood, B.; Pendry, J. B.; Tsai, D. P. Directed subwavelength imaging using a layered metal-dielectric system. *Phys. Rev. B* **2006**, *74* (11), 115116.
(38) Bergman, D. J. The dielectric constant of a composite material—A problem in classical physics. *Phys. Rep.* **1978**, *43* (9), 377−407.
(39) Simovski, C. R.; Belov, P. A.; Atrashchenko, A. V.; Kivshar, Y. S. Wire Metamaterials: Physics and Applications. *Adv. Mater.* **2012**, *24* (31), 4229−4248.
(40) Kuester, E.; Holloway, C. Comparison of approximations for effective parameters of artificial dielectrics. *IEEE Trans. Microwave Theory Technol.* **1990**, *38* (11), 1752−1755.

https://doi.org/10.1021/acsphotonics.5c01105
ACS Photonics XXXX, XXX, XXX−XXX

(41) Müller, U. Die Symmetrie von Spiralketten. *Acta Crystallographica Section B* **2017**, *73* (3), 443−452.
(42) Goshen, S.; Mukamel, D.; Shtrikman, S. A Classification of the Possible Symmetry Groups of Liquid Crystals. *Mol. Cryst. Liq. Cryst.* **1975**, *31* (1−2), 171−184.
(43) de Juan, F.; Grushin, A. G.; Morimoto, T.; Moore, J. E. Quantized circular photogalvanic effect in Weyl semimetals. *Nat. Commun.* **2017**, *8* (1), 15995.
(44) Wu, J.; Zeng, R.; Liang, J.; Huang, D.; Dai, X.; Xiang, Y. Spin-dependent and tunable perfect absorption in a Fabry-Perot cavity containing a multi-Weyl semimetal. *Opt. Express* **2023**, *31* (19), 30079−30091.
(45) Xue, H.; Yang, Y.; Zhang, B. Topological acoustics. *Nat. Rev. Mater.* **2022**, *7* (12), 974−990.
(46) Su, Y.; Wang, X. S.; Wang, X. R. Magnonic Weyl semimetal and chiral anomaly in pyrochlore ferromagnets. *Phys. Rev. B* **2017**, *95* (22), 224403.
(47) Rafi-Ul-Islam, S. M.; Bin Siu, Z.; Jalil, M. B. A. Topoelectrical circuit realization of a Weyl semimetal heterojunction. *Commun. Phys.* **2020**, *3* (1), 72.
(48) Johnson, S. G.; Joannopoulos, J. D. Block-iterative frequency-domain methods for Maxwell's equations in a planewave basis. *Opt. Express* **2001**, *8* (3), 173−190.

https://doi.org/10.1021/acsphotonics.5c01105
ACS Photonics XXXX, XXX, XXX−XXX